Journal of Alloys and Compounds 509 (2011) 5942–5946

Contents lists available at ScienceDirect

Journal of Alloys and Compounds

journal homepage: www.elsevier.com/locate/jallcom

Detailed of X-ray diffraction and photoluminescence studies of Ce doped ZnO nanocrystals

Achamma George [a,*], Suchinder K. Sharma [a,**], Santa Chawla [b], M.M. Malik [a], M.S. Qureshi [a]

[a] Luminescence Laboratory, Dept. of Physics, Maulana Azad National Institute of Technology, Bhopal, India
[b] National Physical Laboratory, New Delhi, India

ARTICLE INFO

Article history:
Received 24 September 2010
Received in revised form 16 February 2011
Accepted 3 March 2011
Available online 11 March 2011

Keywords:
Lanthanide
Photoluminescence
Lattice parameters
Excitons
ZnO

ABSTRACT

Pristine and Ce doped ZnO nanopowders were synthesized by simple refluxing technique. A detailed X-ray diffraction analysis was carried out to evaluate the contribution of dopant ion concentration on strain and lattice parameters. A particle size of 20 nm was obtained via TEM studies. Spherical morphology was obtained for Ce doped ZnO nanocrystals. Multiple emission bands were observed for pristine and doped ZnO samples where, 401 nm emission band corresponds to a contribution due to free excitons recombination through an exciton–exciton collisions. With the Ce addition, the surface defects increases and the emission intensity decreases.

1. Introduction

The varied aspects of luminescence and the complex processes involved in the origin of light emission, offer interesting challenges for researchers in this field. This is one research field, wherein, diverse application area exists which ranges from radiation monitoring for health and safety, lamps and display purposes to X-ray imaging and other means of medical diagnostics. With a direct band gap of 3.37 eV and high exciton binding energy (60 MeV), ZnO offers itself as a suitable candidate for such numerous applications. ZnO holds promises as a material for blue/UV optoelectronics, as an alternative to GaN, as a cheap, transparent, conducting oxide, and as a material for electronic circuits which are transparent in the visible or for the semiconductor spintronics [1].

ZnO possesses unique ability to attain different morphological forms. Earlier, we have already reported wealth of morphological forms for combustion synthesized ZnO powders which include cones and spherulites [2]. In order to extend the domain of our research on ZnO synthesis and to meet the industrial needs of low-cost, large-scale production of ZnO crystals with spherical morphology, herein, we report the synthesis of ZnO nanocrystals via low temperature refluxing technique.

Lanthanide ion doped semiconductor nanoparticles are technologically important, as they have potential applications for making efficient luminescent materials. Generally, lanthanide ions such as Eu^{3+}, Er^{3+}, etc. are incorporated in semiconductors to improve the luminescence efficiency by energy transfer processes. Herein, we have chosen cerium (Ce) as a suitable dopant for ZnO matrix. Ce is the first member of lanthanide series and can possess anomalous emission characteristics (from UV to red region). Such behaviour has already been reported [3]. Different authors have reported the synthesis of ZnO:Ce [4–7]. In these reports, the synthesis was performed via time consuming, expensive procedures. The synthesis temperature and the processing time are the much worried crucial issues in ZnO:Ce synthesis. Based on these observations, the present work is carried out to fulfill two objectives: (a) controlled single step synthesis of spherical ZnO nanocrystals and, (b) influence of Ce^{3+} doping on photoluminescence characteristics. The work pursued includes synthesis of ZnO nanocrystals, studies on their structural and morpho-structural aspects and studies on radiative recombination processes for pristine and doped samples.

2. Experimental

2.1. Synthesis

GR grade (purity >99%) zinc acetate ($Zn(CH_3COO)_2{\cdot}2H_2O$), cerium nitrate ($Ce(NO_3)_3{\cdot}6H_2O$), urea ($CH_2NH_2COOH$), and ethylene glycol ($C_2H_6O_2$), were procured from E. Merck, India. No further purification of precursors was carried out. In a typical experiment, 0.5 g of zinc acetate was dissolved in 50 ml of ethylene glycol.

* Corresponding author. Tel.: +91 755 2670327x1490; fax: +91 755 2670562.
** Corresponding author. Present address: GSDN, Physical Research Laboratory, Ahmedabad, India. Tel.: +91 792 631 4371.
E-mail addresses: gachamma@gmail.com (A. George), suchindersharma@yahoo.co.in (S.K. Sharma).

0925-8388/$ – see front matter © 2011 Elsevier B.V. All rights reserved.
doi:10.1016/j.jallcom.2011.03.017

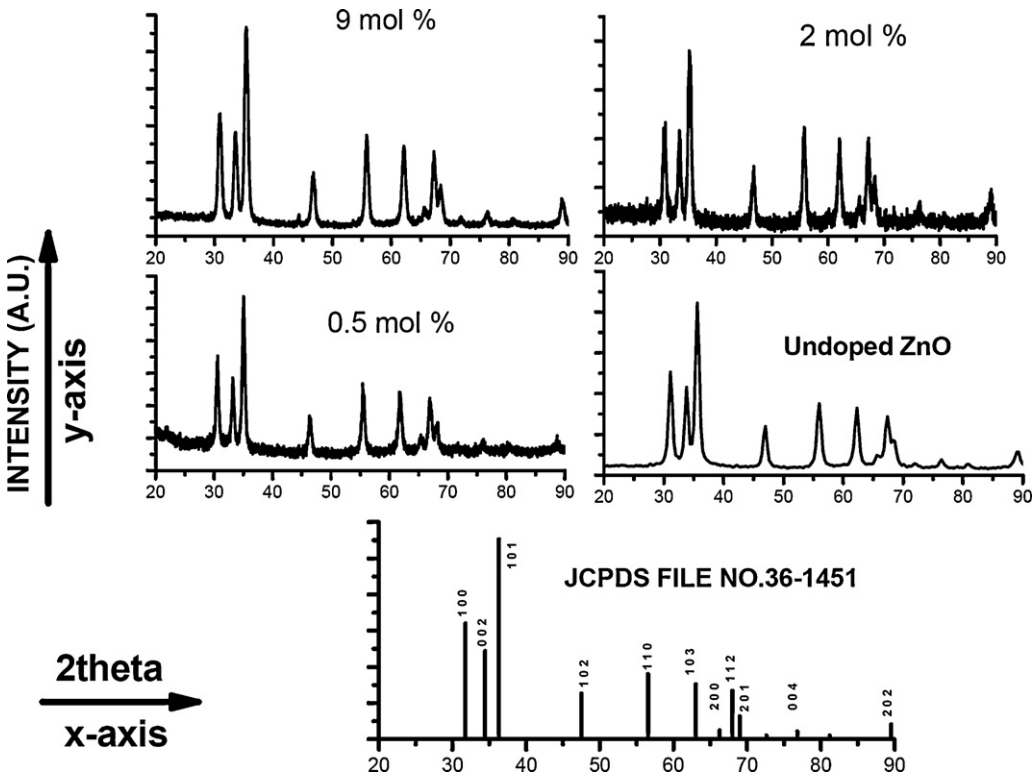

Fig. 1. X-ray diffraction pattern for pristine and Ce doped ZnO nanopowders. The standard data from JCPDS file No. 36-1451 is also shown. No variation in peak positions is observed except few variations in intensities.

Around 1.5 g of urea was added into this solution and the temperature was raised and maintained at 150 °C for 2 h. A white precipitate of ZnO was obtained which was finally separated by centrifugation and washed several times with quadruple distilled water and methanol (to remove trace impurities). The samples were thereafter dried at room temperature. For Ce (0.5–9.0 mol%) doped ZnO nanocrystals, same procedure was followed except, appropriate amount of cerium nitrate was dissolved with the solution at the beginning of the reaction process.

2.2. Characterization

The phase identification of as-synthesized ZnO nanocrystals was performed on Rigaku MiniFlex II instrument with Cu K_α target ($\lambda = 1.54060$ Å) at room temperature. The X-ray generator was operated at 30 kV with a scan speed of 2° min^{-1}. Unit cell parameters were calculated using various utilities in Microsoft Excel. The surface morphology of the as-prepared sample was obtained on JEOL JSM 6390 scanning electron microscope (SEM). TEM measurements were carried out on Philips CM200 instrument with a resolution of 2.4 Å. The photoluminescence spectra were obtained using a Xe-lamp source and Edinburgh Instruments FLSP920 steady state spectrometer.

3. Results and discussion

3.1. XRD results

To ascertain the crystalline nature of pristine and doped ZnO nanocrystalline powders, X-ray diffraction studies were performed. The patterns for the same are shown in Fig. 1 along with standard pattern from Joint committee powder diffraction standards (JCPDS) file no 36-1451. In all the cases, the as-synthesized nanopowders are phase pure and no additional signatures were observed. It is anticipated that the Ce^{3+} has substituted the Zn^{2+} sites due to their matching radii. The peak broadening features in the present case has been assigned to the smaller crystallite size (also confirmed from TEM results). From the 2θ values, the inter-planar spacing 'd' of the peaks is calculated. The least square minimization procedures have been adopted to refine the lattice parameters. The values are listed in Table 1. A good agreement between the observed and the theoretical calculated d values is found to exist and hence, suggests the suitability of unit cell parameters and the crystal structure. It is to be remembered here that, the determination of diffraction pattern from the instrument can include experimental errors due to diffractometer optics. For the sake of pattern indexing, accurate determination of peak positions is essential. For this purpose, the 2θ of the instrument is calibrated using NIST Si standard 640b. The instrument was adjusted to produce a full-width at half maximum for the Si(1 1 1) reflection of 0.1° 2θ.

3.2. Lattice parameters and crystallite size

The variation of lattice parameters with dopant concentrations are tabulated in Table 2. The least square minimization procedures have been adopted to calculate the values. The variation of aspects ratio (c/a) with dopant concentration is shown in Fig. 2. The values are almost constant and has good correlation with the standard value (1.60). The trend suggests that the larger Ce^{3+} ($r_{Ce^{3+}} = 1.03$ Å) is able to substitute the smaller Zn^{2+} ion ($r_{Zn^{2+}} = 0.74$ Å) in the matrix with little or no effect on the overall crystal structure. Also,

Table 1
Comparison of observed and calculated d values (Å) for some of the reflections of ZnO:Ce nanopowders.

h	k	l	$d_{obs.}$	$d_{cal.}$
1	0	0	2.872	2.873
0	0	2	2.654	2.650
1	0	1	2.519	2.520
1	0	2	1.933	1.932
1	1	0	1.644	1.641
1	0	3	1.487	1.489
2	0	0	1.421	1.422
1	1	2	1.389	1.388
2	0	1	1.365	1.367
0	0	4	1.248	1.246
2	0	2	1.095	1.096

Table 2
Variation of lattice parameters and bond length for various dopant ion concentrations.

Ce content (mol%)	*a* or *b*	*c*	*c*/*a*	Bond length '*l*' (Å)
Undoped	3.25	5.22	1.6061	2.0185
0.5	3.27	5.35	1.6360	2.0007
2.0	3.27	5.28	1.6146	2.0307
4.0	3.29	5.28	1.6048	2.0704
6.0	3.26	5.34	1.6380	1.9859
9.0	3.28	5.29	1.6128	2.0459

we expect the substitutional doping to change the bond distances reflected through a change in unit cell lattice parameters. The peak intensities can be affected by the change in electron density due to substitution of atoms. To see the effect of dopant concentration on Zn–O bond length, Eq. (1) is used.

$$l = \sqrt{\left[\frac{a^2}{3} + \left(\frac{3}{4} - \frac{a^2}{3c^2}\right)^2 c^2\right]} \quad (1)$$

where '*l*' is bond length and '*a*' and '*c*' are lattice parameters. The bond lengths have been tabulated in Table 2. It is observed that the variation of bond length with respect to aspect ratio does not follow any particular trend and has mean value of 2.02535 Å. The decrease in lattice parameters can be attributed to replacement of Zn ions with Ce ions while the increase in lattice parameters can be due to interstitial incorporation of Ce ions in ZnO lattice [8]. Hence we anticipate that at low Ce concentrations, interstitial incorporation is favored while at high Ce concentrations, substitution and interstitial substitution are comparable processes.

The integral width of the diffraction peak can be linked to the apparent size of the crystal, micro-strain and defects like stacking faults and dislocations. Crystallite size using XRD patterns is a measure of the size of the coherently diffracting domains and is not generally same as the particle size due to powder aggregates. Strain is defined as the change in length per unit length and is measured as the change in d spacing of a strained sample compared to the unstrained state. The apparent crystallite size can be calculated using Scherrer equation as given in Eq. (2).

$$d = \frac{k\lambda}{\beta \cos\theta} \quad (2)$$

where k is close to unity, θ is Bragg angle of $\{h\,k\,l\}$ reflections, d is volume-weighted quantity and λ is wavelength of X-rays used. The integral breadth of the peaks diffracted by crystals with volume

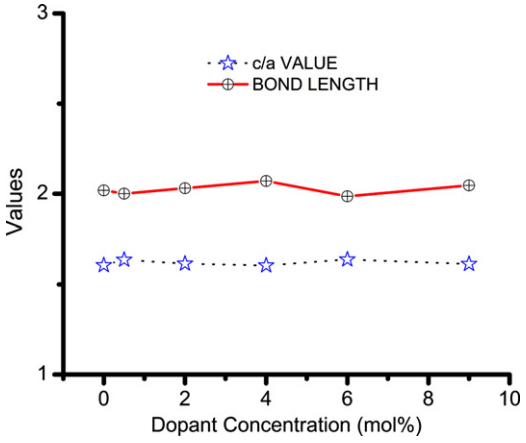

Fig. 2. Variation of lattice parameters (aspect ratio, c/a) and Zn–O bond length with dopant ion concentration for Ce doped ZnO nanopowders.

Table 3
Calculated crystallite size and micro-strain from Williamson–Hall plot for various dopant ion concentrations.

Dopant concentration	Size (nm)	Strain
Undoped	10.23	0.000213 ± 0.0001
0.5	14.21	0.000245 ± 0.0003
2.0	14.36	0.000536 ± 0.0002
4.0	13.21	0.000721 ± 0.0003
6.0	15.21	0.000582 ± 0.0003
9.0	14.98	0.000543 ± 0.0001

defects can be written using Eq. (3).

$$\beta^T = \frac{\lambda}{L\cos\theta} \quad \text{and} \quad \beta^d = \eta \tan\theta \quad (3)$$

With regard due to effect of size (or due to stacking faults, β^T) and widening induced by microstrain (β^d), respectively. But in our case, the contribution could be due to these two factors simultaneously. To calculate these two contributions, Williamson–Hall method [9] is applied.

3.3. Williamson–Hall method

It assumes that the size of the crystal and the presence of crystallographic distortion lead to Lorentzian intensity distribution. If we denote by β_p the pure breadth and by β^T and β^d the breadths related to size and microstrains, respectively, then we obtain Eq. (4).

$$\beta_P = \beta^T + \beta^d \quad (4)$$

Putting values from Eq. (3) in Eq. (4) and considering '*L*' to be Lorentzian function, we have

$$\beta_P = \frac{\lambda}{L\cos\theta} + \eta \tan\theta \quad (5)$$

Or,

$$\frac{\beta_P \cos\theta}{\lambda} = \frac{1}{L} + \eta\frac{\sin\theta}{\lambda} \quad (6)$$

Hence, from the plot between $(\beta\cos\theta)/\lambda$ and $(\sin\theta/\lambda)$, a straight line is obtained with a y-intercept equal to the inverse of size and a slope equal to the value of the micro-strain. The results for the effect of dopant ion concentration on size and strain are tabulated in Table 3. The Williamson–Hall plot for Ce (0.5 mol%) doped sample is shown in Fig. 3. The observation of small micro-strain may be attributed to the electrostatic attraction or repulsion

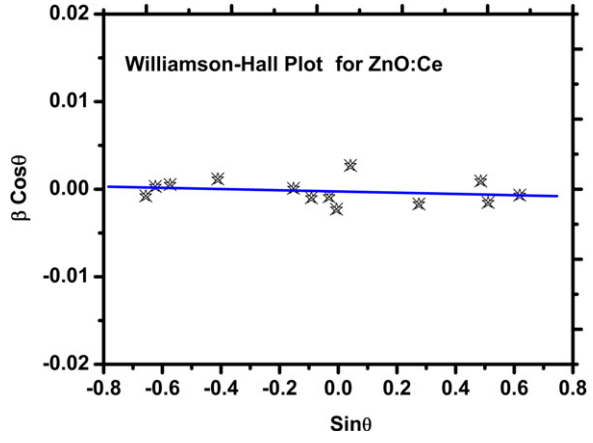

Fig. 3. Williamson–Hall plot for Ce (0.5 mol%) doped ZnO sample to determine size and micro-strain contribution. Strain anisotropy is not considered in the present case.

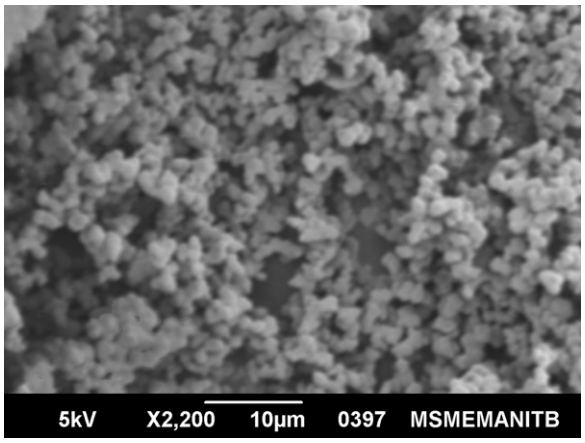

Fig. 4. SEM micrograph for Ce (0.5 mol%) doped ZnO sample. Spherical morphology is obtained and is attributed to the presence of ethylene glycol during synthesis procedure.

between ions along different planes. We realize that the direct mapping of microstructure is possible only after transmission electron microscopy (TEM) or laser based scattering experiments. Therefore, to exactly determine the crystallite size, TEM studies are performed.

3.4. Morphology and TEM results for ZnO nanocrystals

The SEM pattern for Ce (0.5 mol%) doped ZnO nanocrystals is shown in Fig. 4. The crystallites have spherical morphology. There are numerous factors that can affect the shape and size of the crystallites during synthesis procedure. In the present case, we anticipate that the spherical morphology is obtained due to the crucial role played by the ethylene glycol during synthesis of ZnO nanocrystals. As an important non-ionic surfactant with uniform and ordered chain like structure, ethylene glycol is mainly absorbed at the surface of the metal oxides. It is known that the organic ligands with high binding affinities can promote self-assembly driven by the interaction between the surface absorbed ligands instead of between the particles themselves. In addition, the ligands involved self assembly is likely to generate single crystalline architecture that usually could not be obtained from the conventional processes. Hence, we anticipate that during the self assembly, at low concentrations, ZnO particles rotated themselves and aggregated through ethylene glycol while sharing same crystallographic planes leading to spherical morphology.

To confirm the size of the ZnO powders, TEM study was performed. The TEM pattern for 0.5 mol% Ce doped sample is shown in Fig. 5. As noticed, an average crystallite size of 20 nm is approximated in the present case. A good correlation is found to exist between mathematical calculations from XRD analysis and those obtained via TEM studies.

3.5. Photoluminescence results

The emission spectrum of pristine ZnO contains various 5 maxima at 220 nm excitation wavelength (Fig. 6). The bands are present in near-UV and visible regions and are attributed due to the presence of various type of defects in the as-synthesized ZnO. The probable defects can be interstitial Zn or O (Zn_i or O_i), zinc vacancy (V_{Zn}) or the oxygen antisite (O_{Zn}). The emission spectra of most ZnO sample showed a near-band-edge line ($\lambda = 401$ nm, $\Delta\lambda = 19$ nm) followed by a deep level luminescence in lower energy regime ($\lambda = 435$ nm, 467 nm, 558 nm and 599 nm). Higher wavelength band originates from the various defects depending upon the growth technique and can decrease the emission efficiency of the UV

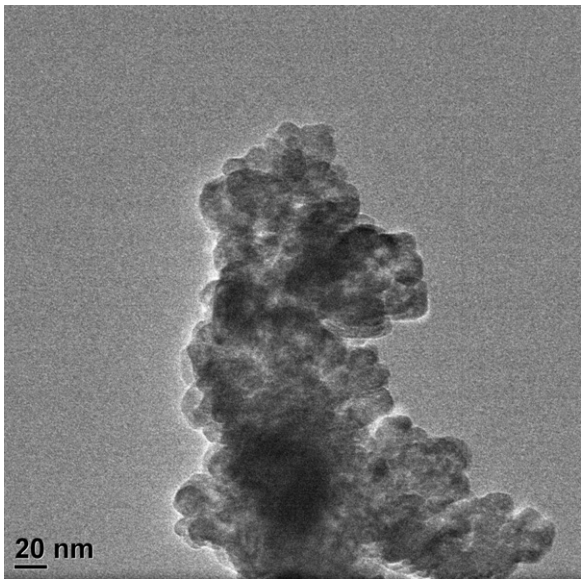

Fig. 5. TEM results for doped ZnO (Ce = 0.5 mol%). The crystallite size is observed to be 20 nm.

emission while increasing the lasing action threshold. Hence, the optical quality is evaluated using intensity ratios between near UV and the green bands. Luminescence features also depend on other crucial factors which includes solvent, atmosphere, starting materials, etc. and is attributed to different processing conditions (quenching centres) during synthesis process. In the present case, the higher energy band (401 nm) is assigned to the occurrence of free excitons' recombination through an exciton–exciton collision process [10]. On the other hand, the lower energy aqua-blue (467 nm) emission band is assigned to the presence of oxygen vacancies or to some type of new defects formed during synthesis of ZnO. The yellow band at 558 nm is thought to have evolved due to transition from shallow donor to a deep acceptor level above the top of the valence band and is tentatively assigned to acceptor involved in V_{Zn} or V_{Zn}^- shallow donor complexes [11]. The red band has been assigned to other type of intermediate trapping state. To exactly claim about the exact nature of defects, further studies like calcining effects (on PL) of ZnO in oxygen or ammonia atmosphere or ESR mapping is required and thus, paves the way for further research.

For Ce doped samples, with the increase in Ce content, the intensity ratio 401 nm/558 nm band is found to increase. When incorporated into any matrix, Ce can attain two states, i.e. Ce^{3+} and Ce^{4+}. f–d transitions are susceptible to field effects and hence, 5d

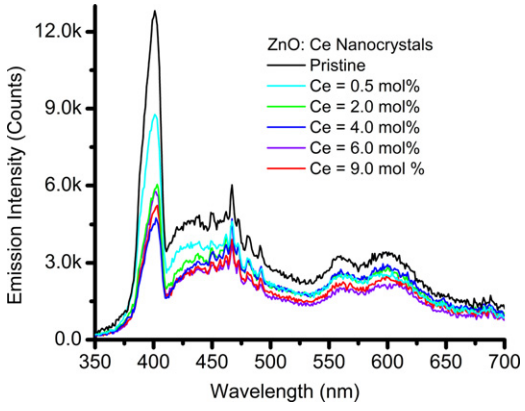

Fig. 6. Photoluminescence emission spectra for pristine and Ce (0.5–9.0 mol%) doped ZnO nanocrystals.

state of Ce^{3+} splits into two states, namely E_g and T_{2g} with broad FWHM characteristics. At higher Ce concentrations (4 and 9 mol%), the emission spectrum maximum at 401 nm is narrow in nature and the red shift is evident. It is anticipated that, as the dopant is incorporated into the host matrix, strain increases. Consequentially, some new type of defects are expected to be formed. The introduced dopant ions might shape a shallow energy level near valence band. Hence, we assign the red shift to the defects and the probable shallower energy levels [12]. With the decrease in emission intensity for the increase in Ce doping, we anticipate that the surface bound states act as defect states leading to high non-radiative relaxation. The decrease in luminescence intensity depends on centre to centre interaction and the distance at which they interact. The spectral overlap of wavefunctions from these energy states can lead to migration of energy in a non-radiative manner leading to decreased intensity. Also, the transport of energy from one centre to another is highly dependent up on the spatial spread of wavefunctions and the extent of overlap. Hence, looking at the present results, we realize the need for further studies like lifetime measurements, neutronic diffraction experiments and EXAFS studies. At this stage, the possibility of formation of new defects along with emission due to Ce^{3+} cannot be neglected. The studies in this direction are in progress.

4. Conclusions

ZnO nanocrystals with spherical morphology have been synthesized via time and money saving refluxing technique for industrial applications. Spherical morphology is designated to the crucial role played by the ethylene glycol during synthesis. With the increase in Ce concentration, the variation in lattice parameters is negligible. Williamson–Hall plot provide crucial values for crystallite size and is approximated at ~15 nm. The value is in good agreement with the TEM results (20 nm). For pristine samples, PL is broad in nature with maxima at various positions in visible region of electromagnetic spectrum. For Ce doped samples, the emission intensity decreases and is anticipated to be due to formation of additional surface defects. The higher wavelength bands are assigned to either emission from Ce lowest band (E_g) or to the formation of some new type of defects during synthesis.

Acknowledgements

The author A.G. owes sincere thanks to director, MANIT, Bhopal for research fellowship and necessary facilities. The authors would also like to thank Prof. R.N. Dubey for his kind support and suggestions. We also thank director, Madhya-Pradesh Centre for Science and Technology (MPCST), RSIC, IIT, Mumbai and NPL, New Delhi for the centrifugation, TEM and PL measurement facilities.

References

[1] C. Klingshirn, Phys. Status Solidi (b) 244 (2007) 3027–3073.
[2] S.K. Sharma, S.S. Pitale, M. Manzar Malik, R.N. Dubey, M.S. Qureshi, S. Ojha, Physica B 405 (2010) 866–874.
[3] S.K. Sharma, S.S. Pitale, M. Manzar Malik, R.N. Dubey, M.S. Qureshi, J. Lumin. 129 (2009) 140–147.
[4] C. Ge, C. Xie, S. Cai, Mater. Sci. Eng. B 137 (2007) 53–58.
[5] L. Fen, Y. Bo, Y. Bo, J. Anxi, S. Chunhong, S. Chunhong, W. Xin, J. Rare Earth 25 (2007) 306–310.
[6] J. Yang, M. Gao, L. Yang, Y. Zhang, J. Lang, D. Wang, Y. Wang, H. Liu, H. Fan, Appl. Surf. Sci. 255 (2008) 2646–2650.
[7] J. Iqbal, X. Liu, H. Zhu, Z.B. Wu, Y. Zhang, D. Yu, R. Yu, Acta Mater. 57 (2009) 4790–4796.
[8] G. Srinivasan, R.T. Rajendra Kumar, J. Kumar, J. Sol–Gel Sci. Technol. 43 (2007) 171–177.
[9] G.K. Williamson, W.H. Hall, Acta Metall. 1 (1953) 22.
[10] C. Karunakaran, P. Gomathisankar, G. Manikandan, Mater. Chem. Phys. 123 (2010) 585–594.
[11] M.A. Reshchikov, H. Morkoc, B. Nemeth, J. Nause, J. Xie, B. Hertog, A. Osinsky, Physics B 401–402 (2007) 358–361.
[12] Y.R. Ryu, T.S. Lee, H.W. White, Appl. Phys. Lett. 83 (2003) 87–89.